Nuclear Inst. and Methods in Physics Research, A 946 (2019) 162691

Contents lists available at ScienceDirect

Nuclear Inst. and Methods in Physics Research, A

journal homepage: www.elsevier.com/locate/nima

Reconfigurable positron annihilation lifetime spectrometer utilizing a multi-channel digitizer

L.H. Cong, B.C. Gu, X.X. Han, Q.H. Zhao, Z.W. Pan, R. Ye, J.Q. Guo, B.J. Ye *

State Key Laboratory of Particle Detection and Electronics, University of Science and Technology of China, Hefei 230026, China

ARTICLE INFO

Keywords:
Positron annihilation spectroscopy
$LaBr_3$
Distortion
Energy spectrum
Monte Carlo simulation

ABSTRACT

Positron annihilation lifetime (PAL) spectroscopy is a powerful tool to study atomic-scaled microstructure of materials. But PAL spectra can be easily distorted, then one will get wrong conclusions. Conventional PAL spectrometers have been widely used but the data processing capability is limited. In order to deal with the generally existed problems related to spectra distortion, and find an economic way to let conventional PAL spectrometers have better performance, we design a reconfigurable PAL spectrometer based on conventional electronic system, multi-channel digitizer card, and $LaBr_3$ scintillator. By using several data processing methods, analysis results of PAL spectra show significant improvements. We discuss the reasons that cause PAL spectra distortion, and try to figure out how our methods can bring changes. Related works including PAL spectra simulation and Geant4 energy deposition simulation have been done. Several other functions such as time walk offset have been developed to improve the performance of whole system. The spectrometer is still capable to add more functions if needed.

1. Introduction

Positron annihilation spectroscopy is an effective technique to study the microstructure of condensed matter, such as lattice deformation [1]. Many relevant techniques have been developed, including positron annihilation lifetime (PAL) spectroscopy, coincidence Doppler broadening (CDB) spectroscopy, angular correlation of annihilation radiation (ACAR), age-momentum correlation (AMOC), and slow positron beam techniques. Among them, PAL spectroscopy is most commonly used, which measuring the "lifetime" between the implanting and decaying time of positrons in samples. A PAL spectrum is the superposition of several exponentially decay lifetime components convoluted with the response function of spectrometer. Special programs need to be used to analyze it [2]. As we know, positron lifetime (τ) in materials can be very short comparing to the time measurement accuracy, and the PAL spectra are easily distorted because of some instrumental reasons [3]. These will lead to incorrect analysis results, especially for the "close" lifetime components with only dozens of picoseconds in difference.

Conventional PAL spectrometer comprises NIM standard electronic modules including constant fraction discriminator (CFD), time-to-amplitude converter (TAC), amplifier, and multichannel analyzer (MCA). In recent years, several groups have developed digital PAL spectrometers, replaced the bulky analog electronic devices with digital oscilloscopes. Digital spectrometer has strong data processing capability to realize more functions and better performance. Some digital PAL spectrometers with time resolution less than 150 ps in FWHM (full width at half maximum) have been reported [4,5]. But it takes many efforts to build a digital spectrometer, and its performance depends on the quality of the oscilloscope which can be quite expensive. It is also impossible to replace all the conventional PAL spectrometers with digital ones in a short time. So we want to add some digital-like functions into the conventional PAL spectrometer [6,7] to diminish spectra distortion and get better performance.

In this work, we develop a PAL spectrometer based on conventional NIM modules (CFD, TAC, amplifier) and commonly used data acquisition equipment [8]. Our goal is to combine the advantages of conventional and digital spectrometers. By using a multi-channel digitizer, both time and energy information of coincidence events are recorded simultaneously for further processing. We try to figure out problems within the spectrometer that causing PAL spectra distortion and incorrect analysis results, then overcome them by software methods. Related simulation works also need to be done to provide more information in theory.

2. Spectrometer design

The hardware structure of our PAL spectrometer is shown in Fig. 1. It is almost the same as conventional fast-fast coincidence system, but a multi-channel digitizer card (ADLink PCI-9846H) is used. This is a 40 MS/s sampling 16-bit 4-CH digitizer inserted in the PCI slot of computer. Three input channels (CH0, CH1, CH2) are connected to TAC

* Corresponding author.
E-mail address: bjye@ustc.edu.cn (B.J. Ye).

https://doi.org/10.1016/j.nima.2019.162691
Received 7 July 2019; Received in revised form 1 September 2019; Accepted 2 September 2019
Available online xxxx
0168-9002/

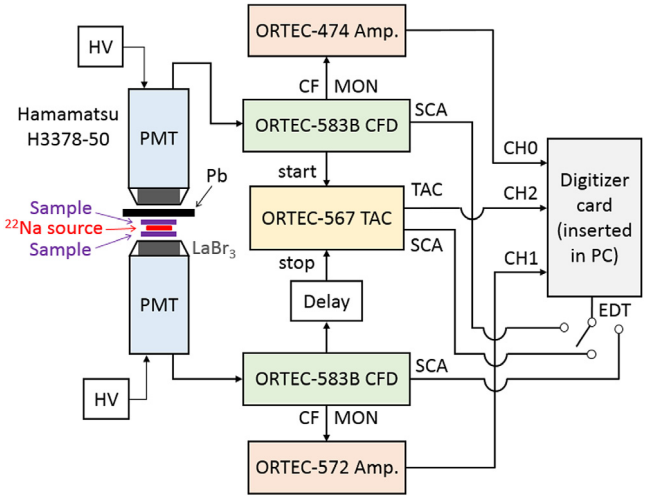

Fig. 1. Block scheme of the positron annihilation lifetime spectrometer.

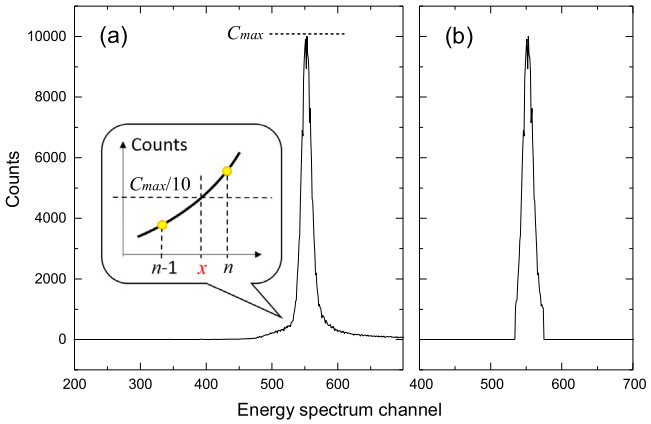

Fig. 2. Software threshold auto setting method. (a) shows the 1275 keV photopeak after setting thresholds by CFD module. We use one-tenth of the maximum value as reference to calculate the "software lower level" x. (b) shows the energy window after setting software thresholds and cutting off "tails".

and amplifier modules, respectively. The external digital trigger (EDT) is connected to the CFD modules firstly to measure energy spectra and set discriminator thresholds. Then the EDT input should be connected to the TAC module for measuring PAL spectra.

We use Hamamatsu H3378-50 photomultipliers (PMT) coupled with $\Phi 25 \times 15$ mm $LaBr_3$:Ce scintillators, powered by ORTEC Model 556 high voltage power supplies (HV). $LaBr_3$ crystal with cerium concentration of 5% provides good energy and time performance for γ-ray detection [9,10]. Our spectrometer can achieve time resolution of about 210 ps and energy resolution of about 5% at 511 keV photopeak. A piece of lead (3-mm-thick) is placed between the sample and start detector to obstruct the backscattering photons [11]. The ^{22}NaCl source is sealed by a pair of Kapton films.

We use electronic modules including ORTEC Model 4001A NIM bin, Model 583B CFD with 15-cm-long delay cable, Model DB463 delay box, Model 567 TAC, Model 474 and Model 572 amplifiers. As H3378-50 PMT has one output (anode), we need to use the CF MON output of CFD module to get energy information [12]. Model 474 timing filter amplifier has short output pulse width comparing to the spectroscopy amplifiers such like Model 572, which reducing pile-up effect. This is quite important at high counting rate.

An energy spectra measuring program was written to set the energy windows. It uses CFD output signals as triggers. One can watch the energy spectra to judge if the CFD thresholds have been well set. But the accuracy of CFD energy discriminator is not very good, especially in SRT (slow rise time) mode. After setting thresholds to select the range of 1275 keV photopeak like Fig. 2(a), there are "tails" on each side of the peak. We can use a reference amplitude, such as one-tenth of the maximum value (C_{max}), to calculate the "software threshold". As shown in Fig. 2(a), the counts of energy spectrum in channel $n-1$ and channel n are a and b, respectively, where $a < C_{max}/10 \leqslant b$. The "software lower level" x can be calculated by

$$\frac{b - C_{max}/10}{C_{max}/10 - a} = \frac{n - x}{x - (n-1)} \tag{1}$$

The upper level can be calculated in the same way. Energy spectrum after cutting "tails" is shown in Fig. 2(b). We can also exclude the distorted amplifier pulses by performing pulse shape discrimination. The software energy windows can be used later when measuring PAL spectra. $LaBr_3$ scintillator's good energy resolution is quite important for this work, so we added FWHM calculation module into the program. Energy resolutions are about 5% for the 511 keV photopeak, and about 3% for the 1275 keV photopeak, which also depend on the counting rate.

Table 1
Software energy window setting methods for a group of PAL spectra measured simultaneously. For either start or stop detector, software thresholds can be set (see Fig. 2) or not.

	Software energy window for start detector	Software energy window for stop detector
Spec. #1	No	No
Spec. #2	No	Yes
Spec. #3	Yes	No
Spec. #4	Yes	Yes

The PAL spectra measuring program was designed reconfigurable. Several PAL spectra can be achieved simultaneously with different on-line data processing methods for comparison. We can set different software thresholds, with or without the "tails" of photopeak (see Fig. 2). This is why we use 3-CH ADC to record both energy and time information. A PAL spectrum has 1024 channels while the channel width is about 25.44 ps. The simultaneously recorded "coincidence energy spectra" may show different shapes compared with the ordinary energy spectra, such as different peak-to-background ratio. This can help us study the reasons of PAL spectra distortion.

3. PAL spectra measurements

When measuring PAL spectra, the EDT input of digitizer card is connected to the TAC module. We set the CFD modules in SRT mode. This can reject slow rising pulses that may cause distortion, but one main disadvantage is the poor energy discriminating accuracy, comparing to the normal CF mode. We just use software to set energy windows, which can significantly improve the energy discriminating accuracy as introduced in Section 2. The amplitude of PMT output pulse is about −1 V for 511 keV energy deposition.

We usually use yttria-stabilized zirconia (YSZ) or single crystal silicon (Si) sample to test our spectrometer. The 9 mol % Y_2O_3 doped YSZ sample, bought from Hefei Kejing Materials Technology Corporation, always shows better performance than Si sample. This is related to its lower lifetime value of about 180 ps [13,14], comparing to that of about 220 ps of Si [15,16]. It is more distinguishable from the source component, i.e. about 385 ps of Kapton film [17,18]. In this work, we also measured a self-made nanocrystal material, 1% aluminum doped zinc oxide (Al-ZnO). It has more than one lifetime component, differing in the analyzing process with YSZ or Si lifetime spectra.

In order to study the effects of different on-line data processing methods, we get a group of 4 PAL spectra numbered from #1 to #4 simultaneously during one measurement. All spectra have the same

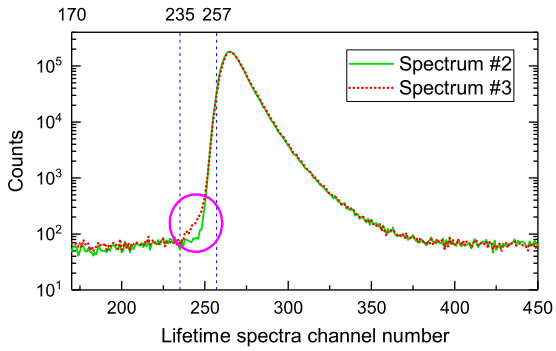

Fig. 3. Two YSZ lifetime spectra measured simultaneously with different software energy windows (refer to Table 1). Difference can be seen on the leading edge of spectral lines.

hardware setting, where the two CFD modules select the energy ranges of 1275 keV and 511 keV photopeaks, respectively. The difference lies in software as shown in Table 1. We use LTv9 program [19] to analyze our spectra. For each spectrum, we decomposed 7 times with different left limits of selected data ranges. Oppositely, the right limit could just be fixed and does not matter. Fig. 3 shows spectra #2 and #3 of one group of YSZ lifetime spectra. Channel 170, 235, and 257 are marked which will be used in Fig. 4. Leading edge distortion [20] can be seen on the spectral line of spectrum #3 but not spectrum #2, because software thresholds for stop detector but not start detector can solve this problem. We will discuss more in Section 4.

The decomposed results of YSZ, Si, and Al-ZnO lifetime spectra are shown in Fig. 4. For YSZ or Si sample, τ_1 should be about 180 or 220 ps ascribed to the sample itself, and τ_2 should be about 385 ps ascribed to the Kapton film of radioactive source. There can be a long lifetime component (τ_3) with intensity less than 1%, which is related to air-gap, NaCl salt, positronium, or something else [21–23]. As can be seen, spectrum #4 shows good results no matter how we select the data range. Spectrum #3 can get reasonable results only if the distorted part (shown in Fig. 3) is excluded, otherwise, the lifetime values would become lower and I_2 would become higher. Spectrum #2 shows stable but incorrect lifetime values. Spectrum #1 combines the disadvantages of spectrum #2 and #3. In a word, the total counts of spectrum #4 is the least (about 2 million), but it shows the best analysis results.

Unlike YSZ or Si, the Al-ZnO sample has two main lifetime components, one of which is not far from the Kapton film's 385 ps. We have to perform source correction first. The source components can be derived from YSZ or Si lifetime spectra. In Fig. 4(c), both lifetime components are ascribed to the Al-ZnO sample itself.

Once we have used Philips XP2020Q PMT to perform the same measurements. That detector was quite aging, but the analysis results of PAL spectra showed the same tendency. So we confirm that the type of detector does not affect our conclusions. Software thresholds for start and stop detectors give distinctive influences to the PAL spectra.

PAL spectra discussed above only used the energy range of photopeak. The Compton plateau was entirely discarded. In order to achieve higher counting rate, we changed the CFD threshold of start detector. The new energy window containing part of the Compton plateau is shown in Fig. 5. We used software to select the Compton edge and 1275 keV photopeak respectively. Two independent PAL spectra with different thresholds were achieved and then combined together. The two independent spectra may show different zero channel positions visibly, which indicate that we should adjust time walk as introduced in the CFD operating manual [24]. Our spectrometer provides an easily used setting method, because we can directly see if the two independent spectra are overlapped (refer to Fig. 3). On the other hand, sometimes it is not easy to solve this problem only by adjusting the CFD modules. If we have got the zero channel positions of both independent spectra, we can diminish their difference by software when combining. Table 2 shows the decomposed results of YSZ lifetime spectra utilizing the new method.

As can be seen from Table 2, spectra A and B show τ_1 of about 170 and 180 ps, respectively, one of which is incorrect. But the combined spectra show τ_1 of nearly 180 ps, not 175 ps (average value). In fact, the biggest difference of two independent spectra lies in the longest lifetime component. Although its intensity is small, it always influences a lot to the decomposition of other parameters. We tried to fix τ_3 by different values when analyzing spectrum A of Table 2. The results are listed in Table 3. As can be seen, the higher that τ_3 is fixed, the higher that τ_1 and τ_2 would be, and I_1 would get lower accordingly. I_3 is quite low (less than 1%), so the statistical error of τ_3 is big and easily influenced by spectra distortion. Signal to noise ratio of Compton plateau is higher than that of photopeak, so the relevant PAL spectra always show more unstable analysis results. If the results can become correct after fixing τ_3 at a reasonable value, we think this is an acceptable operation for PAL spectra analysis.

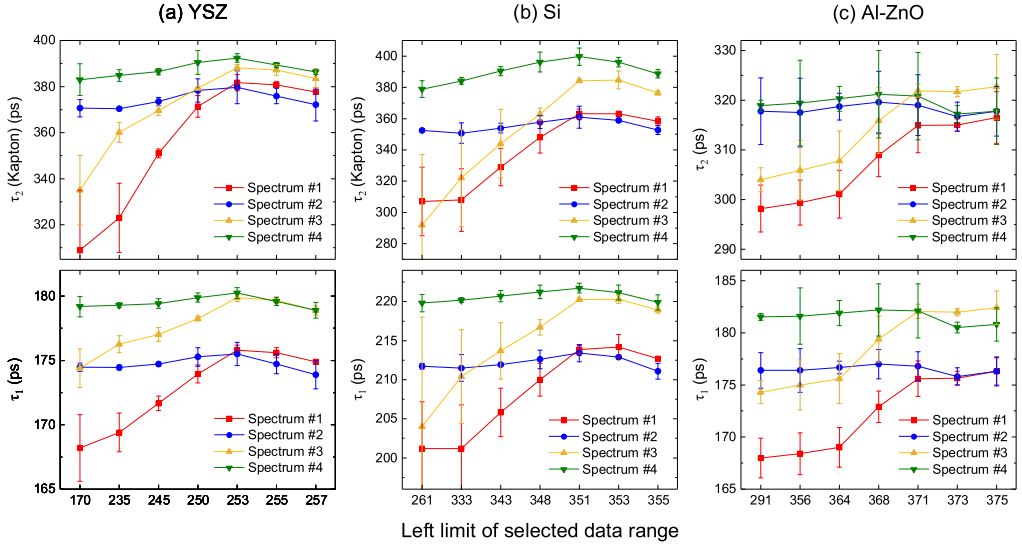

Fig. 4. Decomposed results (τ_1 and τ_2) of YSZ, Si, and Al-ZnO lifetime spectra. For each sample, we got 4 spectra simultaneously with different energy windows (see Table 1). For each spectrum, we decomposed 7 times with different left limits of data ranges. When analyzing YSZ and Si spectra, the Kapton film covered ^{22}NaCl source were just regarded as part of the sample. But source components were fixed when analyzing Al-ZnO spectra. The same tendency of lifetime value τ can be seen for each sample.

Table 2
Decomposed results of YSZ lifetime spectra with different start energy windows. C and D: combination of Compton plateau and photopeak. For spectrum D we performed zero channel offset, the difference of two sub-spectra was diminished.

Spec.	Start energy window	Counts	τ_1 (ps)	I_1 (%)	τ_2 (ps)	I_2 (%)	τ_3 (ps)	I_3 (%)
A	Compton plateau	1183919	170.8 ± 1.2	73.9 ± 1.2	320.9 ± 8.4	24.7 ± 1.2	922 ± 27	1.37 ± 0.13
B	1275 keV photopeak	1000000	180.5 ± 1.6	82.7 ± 0.8	387.7 ± 8.0	16.9 ± 0.8	1910 ± 130	0.388 ± 0.032
C	Combination	2183919	178.4 ± 1.5	81.2 ± 1.0	370 ± 10	18.3 ± 1.0	1370 ± 100	0.571 ± 0.084
D	Combination	2183919	179.9 ± 1.5	82.2 ± 1.0	378 ± 11	17.3 ± 1.0	1440 ± 160	0.517 ± 0.093

τ_2 and τ_3 refer to the source components.

Table 3
Decomposed results of spectrum A shown in Table 2 with different τ_3 values. Component 3 only shares a low intensity but can influence a lot.

τ_3 (ps)	I_3 (%)	τ_1 (ps)	I_1 (%)	τ_2 (ps)	I_2 (%)	Fit's variance
600 (fixed)	4.99 ± 0.23	134.7 ± 6.5	32.3 ± 2.4	227.2 ± 2.4	62.7 ± 2.4	1.1172
922 ± 41	1.37 ± 0.18	170.8 ± 3.0	73.9 ± 2.0	321 ± 12	24.7 ± 2.0	1.0879
1000 (fixed)	1.11 ± 0.06	172.7 ± 2.0	76.2 ± 1.4	333.5 ± 8.4	22.7 ± 1.4	1.0867
1500 (fixed)	0.48 ± 0.02	178.7 ± 1.0	82.3 ± 0.7	380.7 ± 5.8	17.2 ± 0.7	1.1035
2000 (fixed)	0.32 ± 0.02	181.0 ± 1.1	84.3 ± 0.7	402.4 ± 8.0	15.4 ± 0.7	1.1226
3000 (fixed)	0.23 ± 0.02	183.1 ± 1.1	86.0 ± 0.6	424.0 ± 7.9	13.8 ± 0.6	1.1506
6000 (fixed)	0.23 ± 0.02	184.9 ± 1.0	87.3 ± 0.5	444.1 ± 7.7	12.4 ± 0.5	1.1862
–	0	188.1 ± 0.7	89.6 ± 0.3	482.3 ± 6.8	10.4 ± 0.3	1.2873

The results with unfixed τ_3 are not completely equal to what were shown in Table 2 because of decomposing uncertainty.

Table 4
Decomposed results of simulated YSZ lifetime spectra with different rates of B-type wrong coincidence events (see Fig. 6) and 10 million counts. τ_3 is fixed at 1.6 ns. τ_1 and τ_2 should be about 180 ps and 385 ps, respectively.

B-type events (%)	τ_1 (ps)	I_1 (%)	τ_2 (ps)	I_2 (%)
0	180.4 ± 0.2	85.1 ± 0.1	384.8 ± 1.0	14.6 ± 0.1
0.5	179.3 ± 0.2	84.74 ± 0.06	383.0 ± 0.5	14.96 ± 0.06
1	178.8	84.61 ± 0.09	381.4 ± 1.6	15.09 ± 0.09
2	177.0 ± 0.1	83.63 ± 0.09	372.7 ± 0.8	16.06 ± 0.09
3	176.8	84.25 ± 0.03	377.6 ± 0.5	15.45 ± 0.03
5	174.3	83.32 ± 0.06	370.0 ± 1.0	16.38 ± 0.06
10	169.8	82.48 ± 0.03	360.5 ± 0.6	17.20 ± 0.03

4. Simulations and discussions

In order to figure out the reasons of PAL spectra distortion, we designed a PAL spectra Monte Carlo simulation program. The lifetime components, time resolution function, and uniform background are produced by exponential, normal, and uniform random value generators, respectively. Parameters including lifetime values and intensities, background rate, time resolution, and channel width are just got from the measured PAL spectra. We can simulate enough counts to keep good statistics [25], and repeat one simulation for several times without changing any parameters. We can add "wrong coincidence events" to the simulated PAL spectra based on several mathematical models, then the distorted spectra will show incorrect analysis results just like the measured spectra.

A coincidence event can occur in several modes as shown in Fig. 6. A-type refers to the "right events" when the two detectors get 1275 keV nuclear photon and 511 keV annihilation photon, respectively. B-type means that energy deposition in start detector comes from both nuclear photon and annihilation photon [26]. C-type means that stop signal is created by the backscattering nuclear photon. There are some more complex coincidence types that we do not show here. If one PMT pulse comes from two or more photons with time difference far less than the pulse width, timing output can be approximately calculated by energy-weighted average method [27]. For an event with lifetime of t_0, the timing output would just be t_0 when A-type coincidence occurs (neglect the time resolution). But when B-type coincidence occurs, the timing output would be about $t_0 \times 764/(511+764) = 0.6 \times t_0$. When C-type coincidence occurs, that would be about $t_0 \times (-1) \times 511/(511+764) = -0.4 \times t_0$. The values in Fig. 6 such like "764" should not be regarded as definite values, because the energy window is a range but not a fixed value. Here we use "764" only for calculation convenience.

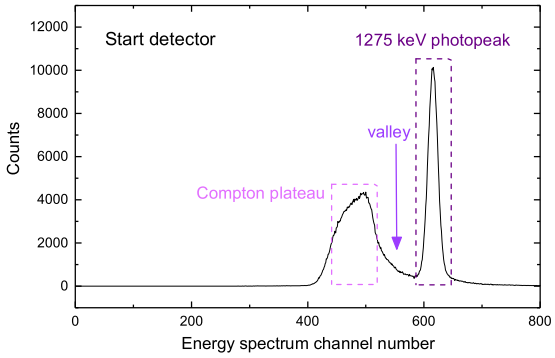

Fig. 5. Energy spectrum of start detector (^{22}Na) after setting CFD thresholds. The "valley" always contain many "incorrect" events, so we discard this part by software when measuring PAL spectra.

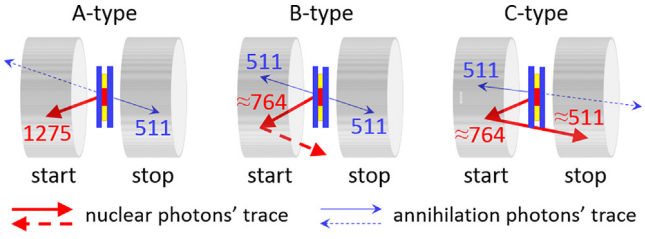

Fig. 6. Three main types of coincidence events. A-type refers to the "right" events. B-type and C-type refer to the "wrong" events. Solid arrows mean gamma photons lose energy in scintillator by the marked values (keV). Dashed arrows mean gamma photons pass through the scintillator.

We simulated a series of YSZ lifetime spectra containing source components. Each spectrum has three lifetime components with mean values (τ) of 180 ps, 385 ps, and 1600 ps, respectively, accounting for 85%, 14.7%, and 0.3%, respectively. According to the energy-weighted average timing model, we added B-type coincidence events by different rates, from 0 to 10%. Each spectrum has 10 million counts with background rate of 1.5% distributed in a range of about 22 ns. The channel width is 25.44 ps and the time resolution is 210 ps in FWHM. Table 4 shows the decomposed results. As can be seen, the more B-type events we added, the lower that τ_1 and τ_2 would be. This is because B-type coincidence events provide "discounted" lifetime values. In experiment, the precise software energy window can diminish B-type

Table 5
Geant4 simulation results of different coincidence types (see Fig. 6) based on our detectors. The energy windows can be set wider or narrower. Wider energy window corresponds to the measured spectra only set CFD thresholds. Narrower energy window corresponds to the measured spectra after setting software thresholds.

Start energy window (keV)	Stop energy window (keV)	Counts	A-type rate (%)	B-type rate (%)	C-type rate (%)	Other rate (%)
[1100, 1450]	[400, 600]	223266	80.926	17.010	0.005	2.059
[1100, 1450]	[487, 535]	205232	80.739	17.197	0.003	2.061
[1237, 1313]	[400, 600]	160492	94.528	5.339	0.002	1.315
[1237, 1313]	[487, 535]	147511	94.426	5.440	0.001	1.322

The energy windows are shown as $[E_a, E_b]$, where E_a is the lower level, and E_b is the upper level.

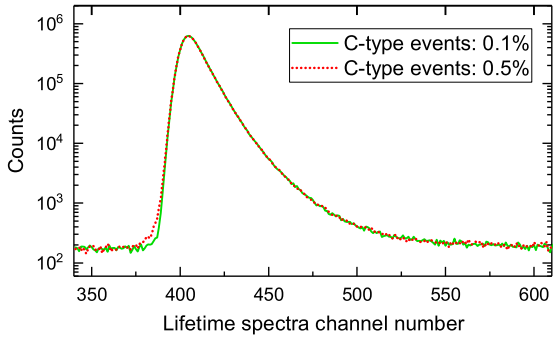

Fig. 7. Simulated YSZ lifetime spectra with C-type wrong coincidence events (see Fig. 6) of 0.1% and 0.5%, respectively. Leading edge distortion can be seen just like the measured spectra shown in Fig. 3.

events. We think this is why software threshold setting for start detector can significantly improve the performance of measured PAL spectra.

Then we simulated a series of YSZ lifetime spectra added different rates of C-type coincidence events, from 0 to 0.5%. According to the energy-weighted average timing model, this provides events with "negative" lifetime values. Fig. 7 shows the simulated PAL spectra added C-type events of 0.1% and 0.5%. Leading edge distortion can be seen just the same as Fig. 3. Decomposed results of these spectra would be significantly influenced by data range selection. This is why we usually do not select too many points on the leading edge of measured PAL spectra for analysis. In experiments, C-type events are caused by γ-ray backscattering. We think software threshold setting for stop detector (maybe also start detector) can solve this problem.

We have simulated several PAL spectra with different wrong coincidence events, but still do not know if those kinds of events really exist in the measured spectra. So we use Geant4 simulation toolkit [28] to study the energy deposition in scintillators. According to our model, positrons emitted by ^{22}Na radioactive source annihilate in Si sample. Radius of the source spot is 1 mm. γ-ray can interact with materials by photoelectric effect, Compton scattering, pair production, or Rayleigh scattering. Distance between the back-to-back detectors is 1 cm. The ^{22}Na source is put 6.5 mm away from the central axis of detectors. We record energy deposition of three photons (two 511 keV and one 1275 keV) in both detectors separately to judge the coincidence type. Gaussian distributed energy resolution function was added. Square of FWHM is proportional to the energy and the energy resolution is set to be 5% for 511 keV. 800 million decay events were simulated. The rates of each coincidence type are shown in Table 5.

According to the Geant4 simulation results, there is a significant positive correlation between the rate of B-type events and the energy window width of start detector. This meets our expectation. But the rates of C-type events seem too low, we think there are two main reasons. Firstly, the simulation of γ-ray elastic scattering may be not very accurate, which influences the events related to backscattering. Secondly, the "C-type like" events in measured PAL spectra can be caused by some factors other than backscattering, such as pile-up effect. They can also be overcome by software threshold methods but are not considered in our simulation [29]. Now we can only get some qualitative conclusions from these simulation works. In the next step, we will combine the simulation of PAL spectra and energy deposition. Influences of pile-up effect and electronic noise would also be considered.

5. Summary

In this work, we have designed a PAL spectrometer based on commonly used multi-channel digitizer card and conventional NIM standard modules, thus achieve many digital-like functions. The program is designed reconfigurable, several PAL spectra can be achieved simultaneously with different data processing methods. PAL spectra distortion is diminished and the counting rate is guaranteed, which fully take advantage of the good energy resolution of $LaBr_3$ scintillator. Several functions have been developed including software thresholds automatic setting, distorted amplifier pulse exclusion, CFD time walk monitoring and offset, and so on. PAL spectra of typical materials have been measured to test our spectrometer. Some issues of PAL spectra analysis have been discussed. We have also studied the reasons of PAL spectra distortion, then used PAL spectra simulating and Geant4 energy deposition simulating methods to get more proofs. The experience we got from this work is also valuable for other kinds of PAL spectrometers.

Declaration of competing interest

The authors declare that they have no known competing financial interests or personal relationships that could have appeared to influence the work reported in this paper.

Acknowledgments

This work was supported by the National Natural Science Foundation of China (Grant Nos. 11775215 and 11875248). The authors would like to thank Prof. Liang Hao and Dr. An Ran for their help on instrumental and electronic issues.

References

[1] J. Čížek, Characterization of lattice defects in metallic materials by positron annihilation spectroscopy: A review, J. Mater. Sci. Technol. 34 (2018) 577–598, http://dx.doi.org/10.1016/j.jmst.2017.11.050.

[2] B. Gu, W. Zhang, J. Liu, H. Zhang, B. Ye, Accurate and informative analysis of positron annihilation lifetime spectra by using Markov chain Monte-Carlo Bayesian inference method, Nucl. Instrum. Methods Phys. Res. A 928 (2019) 37–42, http://dx.doi.org/10.1016/j.nima.2019.02.056.

[3] L. Dorikens-Vanpraet, D. Segers, M. Dorikens, The influence of geometry on the resolution of a positron annihilation lifetime spectrometer, Appl. Phys. 23 (1980) 149–152, http://dx.doi.org/10.1007/BF00899710.

[4] H. Saito, Y. Nagashima, T. Kurihara, T. Hyodo, A new positron lifetime spectrometer using a fast digital oscilloscope and BaF_2 scintillators, Nucl. Instrum. Methods Phys. Res. A 487 (2002) 612–617, http://dx.doi.org/10.1016/S0168-9002(01)02172-6.

[5] F. Bečvář, J. Čížek, I. Procházka, J. Janotová, The asset of ultra-fast digitizers for positron-lifetime spectroscopy, Nucl. Instrum. Methods Phys. Res. A 539 (2005) 372–385, http://dx.doi.org/10.1016/j.nima.2004.09.031.

[6] T. Sharshar, M.L. Hussein, An optimization of energy window settings for positron annihilation lifetime spectrometers, Nucl. Instrum. Methods Phys. Res. A 546 (2005) 584–590, http://dx.doi.org/10.1016/j.nima.2005.02.045.

[7] D. Bosnar, Z. Kajcsos, L. Liszkay, L. Lohonyai, P. Major, S. Bosnar, C. Kosanović, B. Subotić, Digitized positron lifetime spectrometer for the simultaneous recording of time and energy information, Nucl. Instrum. Methods Phys. Res. A 581 (2007) 91–93, http://dx.doi.org/10.1016/j.nima.2007.07.035.

[8] W. Kong, C.Y. Xi, B.J. Ye, H.M. Weng, X.Y. Zhou, R.D. Han, A digital measurement system of 2-detector Doppler broadening, Nucl. Instrum. Methods Phys. Res. 225 (2004) 623–627, http://dx.doi.org/10.1016/j.nimb.2004.06.006.

[9] K.S. Shah, J. Glodo, M. Klugerman, W.W. Moses, S.E. Derenzo, M.J. Weber, $LaBr_3$:Ce scintillators for gamma ray spectroscopy, 2002 IEEE Nuclear Science Symposium Conference Record, 2002, Norfolk, VA, USA, http://dx.doi.org/10.1109/TNS.2003.820614.

[10] J.H. Liu, D.W. Li, Z.M. Zhang, B.Y. Wang, T.B. Zhang, J. Hao, L. Wei, Using a $LaBr_3$:Ce scintillator for positron annihilation lifetime spectroscopy, Chin. Phys. C 36 (4) (2012) 380–383, http://dx.doi.org/10.1088/1674-1137/36/4/016.

[11] F. Bečvář, J. Čížek, I. Procházka, High-resolution positron lifetime measurement using ultra fast digitizers Acqiris DC211, Appl. Surf. Sci. 255 (2008) 111–114, http://dx.doi.org/10.1016/j.apsusc.2008.05.184.

[12] K. Kosev, M. Butterling, W. Anwand, T. Cowan, A. Hartmann, K. Heidel, M. Jungmann, R. Krause-Rehberg, R. Massarczyk, K.D. Schilling, et al., Evaluation of a microchannel-plate PMT as a potential timing detector suitable for positron lifetime measurements, Nucl. Instrum. Methods Phys. Res. A 624 (2010) 641–645, http://dx.doi.org/10.1016/j.nima.2010.09.131.

[13] X. Guo, Z. Wang, Effect of Niobia on the defect structure of yttria-stabilized zirconia, J. Eur. Ceramic Soc. 18 (1998) 237–240, http://dx.doi.org/10.1016/S0955-2219(97)00123-4.

[14] O. Melikhova, J. Kuriplach, J. Čížek, I. Procházka, W. Anwand, G. Brauer, T.E. Konstantinova, I.A. Danilenko, Positron annihilation in three zirconia polymorphs, Phys. Status Solidi c 4 (10) (2007) 3831–3834, http://dx.doi.org/10.1002/pssc.200675858.

[15] M.J. Puska, R.M. Nieminen, Theory of positrons in solids and on solid surfaces, Rev. Modern Phys. 66 (3) (1994) 841, http://dx.doi.org/10.1103/revmodphys.66.841.

[16] J. Nissilä, K. Rytsölä, R. Aavikko, A. Laakso, K. Saarinen, P. Hautojärvi, Performance analysis of a digital positron lifetime spectrometer, Nucl. Instrum. Methods Phys. Res. A 538 (2005) 778–789, http://dx.doi.org/10.1016/j.nima.2004.08.102.

[17] N. Djourelov, M. Misheva, Source correction in positron annihilation lifetime spectroscopy, J. Phys.: Condens. Matter 8 (1996) 2081–2087, http://dx.doi.org/10.1088/0953-8984/8/12/020.

[18] G. Kanda, L. Ravelli, B. Löwe, W. Egger, D. Keeble, Positron annihilation lifetime spectroscopy study of Kapton thin foils, J. Phys. D: Appl. Phys. 49 (2016) 025305, http://dx.doi.org/10.1088/0022-3727/49/2/025305.

[19] J. Kansy, Microcomputer program for analysis of positron annihilation lifetime spectra, Nucl. Instrum. Methods Phys. Res. A 374 (1996) 235–244, http://dx.doi.org/10.1016/0168-9002(96)00075-7.

[20] F. Bečvář, Methodology of positron lifetime spectroscopy: Present status and perspectives, Nucl. Instrum. Methods Phys. Res. 261 (2007) 871–874, http://dx.doi.org/10.1016/j.nimb.2007.03.042.

[21] S. Charles, J. Tumosa, N. Blair, J.A. Hans, The interactions of positrons with defects in sodium chloride crystals, J. Phys. Chem. 75 (13) (1971) 2030, http://dx.doi.org/10.1021/j100682a021.

[22] T.E.M. Staab, B. Somieski, R. Krause-Rehberg, The data treatment influence on the spectra decomposition in positron lifetime spectroscopy Part 2: The effect of source corrections, Nucl. Instrum. Methods Phys. Res. A 381 (1996) 141–151, http://dx.doi.org/10.1016/0168-9002(96)00585-2.

[23] X. Ning, X. Cao, C. Li, D. Li, P. Zhang, Y. Gong, R. Xia, B. Wang, L. Wei, Modification of source contribution in PALS by simulation using geant4 code, Nucl. Instrum. Methods Phys. Res. 397 (2017) 75–81, http://dx.doi.org/10.1016/j.nimb.2017.02.038.

[24] Advanced Measurement Technology, Inc., Model 583B Constant Fraction Differential Discriminator Operating Manual, D Edition, 2009.

[25] B. Somieski, T.E.M. Staab, R. Krause-Rehberg, The data treatment influence on the spectra decomposition in positron lifetime spectroscopy Part 1: On the interpretation of multi-component analysis studied by Monte Carlo simulated model spectra, Nucl. Instrum. Methods Phys. Res. A 381 (1996) 128–140, http://dx.doi.org/10.1016/0168-9002(96)00584-0.

[26] H. Rajainmäki, High-resolution positron lifetime spectrometer with BaF_2 scintillators, Appl. Phys. A 42 (1987) 205–208, http://dx.doi.org/10.1007/BF00620601.

[27] L.Y. Dubov, V.I. Grafutin, Y.V. Funtikov, Y. Shtotsky, L.V. Elnikova, Optimization of BaF_2 positron-lifetime spectrometer geometry based on the Geant4 simulations, Nucl. Instrum. Methods Phys. Res. 334 (2014) 81–87, http://dx.doi.org/10.1016/j.nimb.2014.05.006.

[28] S. Agostinelli, J. Allison, K. Amako, J. Apostolakis, H. Araujo, P. Arce, M. Asai, D. Axen, S. Banerjee, G. Barrand, et al., Geant4–a simulation toolkit, Nucl. Instrum. Methods Phys. Res. A 506 (2003) 250–303, http://dx.doi.org/10.1016/S0168-9002(03)01368-8.

[29] E.W. Bodnaruk, Design and implementation of a digital positron annihilation lifetime spectrometer for measurements in graphite (Master's thesis), North Carolina State University, Raleigh, North Carolina, USA, 2008.